Original Article | Thoracic Imaging

eISSN 2005-8330
https://doi.org/10.3348/kjr.2024.0472
Korean J Radiol 2024;25(9):833-842

Korean Journal of Radiology
KJR

Deep Learning-Based Reconstruction Algorithm With Lung Enhancement Filter for Chest CT: Effect on Image Quality and Ground Glass Nodule Sharpness

Min-Hee Hwang[1], Shinhyung Kang[2], Ji Won Lee[1], Geewon Lee[1]

[1]Department of Radiology and Medical Research Institute, Pusan National University Hospital, Pusan National University School of Medicine, Busan, Republic of Korea
[2]GE HealthCare, Seoul, Republic of Korea

Objective: To assess the effect of a new lung enhancement filter combined with deep learning image reconstruction (DLIR) algorithm on image quality and ground-glass nodule (GGN) sharpness compared to hybrid iterative reconstruction or DLIR alone.
Materials and Methods: Five artificial spherical GGNs with various densities (-250, -350, -450, -550, and -630 Hounsfield units) and 10 mm in diameter were placed in a thorax anthropomorphic phantom. Four scans at four different radiation dose levels were performed using a 256-slice CT (Revolution Apex CT, GE Healthcare). Each scan was reconstructed using three different reconstruction algorithms: adaptive statistical iterative reconstruction-V at a level of 50% (AR50), Truefidelity (TF), which is a DLIR method, and TF with a lung enhancement filter (TF + Lu). Thus, 12 sets of reconstructed images were obtained and analyzed. Image noise, signal-to-noise ratio, and contrast-to-noise ratio were compared among the three reconstruction algorithms. Nodule sharpness was compared among the three reconstruction algorithms using the full-width at half-maximum value. Furthermore, subjective image quality analysis was performed.
Results: AR50 demonstrated the highest level of noise, which was decreased by using TF + Lu and TF alone (P = 0.001). TF + Lu significantly improved nodule sharpness at all radiation doses compared to TF alone (P = 0.001). The nodule sharpness of TF + Lu was similar to that of AR50. Using TF alone resulted in the lowest nodule sharpness.
Conclusion: Adding a lung enhancement filter to DLIR (TF + Lu) significantly improved the nodule sharpness compared to DLIR alone (TF). TF + Lu can be an effective reconstruction technique to enhance image quality and GGN evaluation in ultralow-dose chest CT scans.
Keywords: Deep learning; Phantoms, imaging; Solitary pulmonary nodule; Multidetector computed tomography

INTRODUCTION

Today, artificial intelligence is one of the most popular fields in medical imaging research. Consequently, several CT vendors and software companies have released deep learning image reconstruction (DLIR) algorithms in recent years [1]. Compared to hybrid iterative reconstructions, DLIR has been reported for its ability to lower radiation doses while maintaining diagnostic image quality due to improved noise reduction [1]. However, a study by Nam et al. [2] revealed that a vendor-specific DLIR produced the least amount of noise and better signal-to-noise ratio (SNR), but also showed image blurring at edge areas. Another study suggested that there is a possibility of decreased spatial resolution when DLIR is used for image reconstruction of examinations performed at very low radiation dose levels [3].

The relatively short examination time combined with the excellent spatial resolution has made CT an invaluable tool for evaluating lung lesions, and in particular, low-dose chest CT has been established as a screening tool for

Received: May 18, 2024 **Revised:** July 4, 2024
Accepted: July 18, 2024
Corresponding author: Geewon Lee, MD, PhD, Department of Radiology and Medical Research Institute, Pusan National University Hospital, Pusan National University School of Medicine, 179 Gudeok-ro, Seo-gu, Busan 49241, Republic of Korea
• E-mail: rabkingdom@naver.com

lung cancers [4]. Furthermore, current nodule guidelines also suggest a low-radiation CT technique for monitoring of lung nodules [5,6]. Consequently, lung nodules, particularly those exhibiting ground-glass characteristics, are frequently detected at low-dose chest CT scans [4]. Ground-glass nodules (GGNs) are defined as an area of increased attenuation that does not completely obscure the underlying bronchial and vascular structures [7]. This imaging finding is nonspecific and encompasses a variety of benign and malignant lesions, such as inflammation, infection, fibrosis, and a lepidic pattern of adenocarcinoma [8]. Apart from nodule size or growth, it has been confirmed that GGNs showing well-defined margins, lobulation, spiculation, and pleural indentation are more likely to be neoplastic lesions [9-11]. As a result, the presence of blotchy patterns or blurred images around the edges of GGNs on DLIR algorithm images could hold significant importance in assessing and monitoring GGNs.

Recently, a vendor released a lung enhancement filter (Lu) that can be applied to DLIR (Truefidelity [TF]). However, its effect on image quality and GGN margins, especially at ultralow-dose radiation, has not been evaluated. Therefore, this study aimed to assess the effect of a new lung enhancement filter combined with the DLIR algorithm on image quality and GGN sharpness compared to hybrid iterative reconstruction or DLIR alone.

MATERIALS AND METHODS

This study did not require Institutional Review Board approval because it did not involve any human participants or animal subjects.

Anthropomorphic Chest Phantom and Synthetic Lung Nodules

We used a multipurpose anthropomorphic chest phantom (LUNGMAN; Kyoto Kagaku Co., Kyoto, Japan) for the study. This phantom measured the same as a male human's thorax, complete with pulmonary vessels and bronchi. Five GGNs with a spherical shape and 10-mm diameter were randomly placed in the phantom using double-sided tape. The GGNs had densities of -250, -350, -450, -550, and -630 Hounsfield units (HU).

CT Image Acquisition and Image Reconstruction Algorithms

All CT images were obtained using a 256-slice CT scanner (Revolution Apex CT, GE Healthcare, Milwaukee, WI, USA). Four separate scans were performed, each with a different radiation dose level (standard, 120 kVp/25 mAs, 100 kVp/15 mAs, and 80 kVp/5 mAs). The standard protocol was performed at 120 kVp, and automated tube current modulation was regulated by the noise index set at a level of 20. All other CT parameters were fixed: collimation, 80 mm; slice thickness, 1.25 mm; pitch, 1.531; and rotation time, 0.35 seconds.

To measure the radiation exposure, the volume of the CT dose index and dose length-product (DLP), which were provided by the scanner system, were recorded. The effective radiation dose of each protocol was calculated by multiplying the DLP by the region-specific conversion coefficient κ of 0.014 mSv/mGy·cm [12].

Each scan was reconstructed using three different reconstruction methods: adaptive statistical iterative reconstruction-V at a level of 50% (AR50), TF at medium level, and TF at medium level combined with a lung enhancement filter (TF + Lu). AR50 was reconstructed using a lung (sharp) kernel, while TF and TF + Lu were reconstructed using a standard kernel. Thus, a total of 12 sets of reconstructed images were obtained and analyzed. The reconstruction slice thickness was 1.25 mm. All reconstructed images were transferred to a dedicated workstation (Advantage Workstation 3.2, GE Healthcare) suitable for postprocessing and analysis of the CT images.

Objective Image Quality Assessment

A scientist with expertise in CT techniques placed 20 circular 0.28-cm^2 regions of interest (ROIs) for each of the airway, pulmonary vessel, fat tissue, and muscle on axial images under the supervision of a thoracic radiologist (with 16 years of experience), i.e., 20 ROIs for the airway, 20 ROIs for pulmonary vessels, 20 ROIs for fat tissue, and 20 ROIs for muscles. The 20 ROIs for the airway were placed along the trachea. For other tissues, 3 ROIs (one for a pulmonary vessel, one for fat tissue, and one for muscle) were placed on each of 20 different axial slices. Thus, there were a total of 80 ROIs in one image dataset. The scientist was blinded to the reconstruction methods, and all 80 ROIs were consistently positioned in identical locations (copied and pasted) across all 12 image sets. We obtained the mean attenuation (MA) and standard deviation (SD) from each ROI.

First, image noise was evaluated using SD values measured from the ROIs placed in the fat tissue. Second, the SNR was calculated at 20 ROIs in the airway and 20

https://doi.org/10.3348/kjr.2024.0472

Korean Journal of Radiology
KJR

ROIs in the vessel using the following equation: SNR = (CT Airway MA/CT Airway SD) and (CT Vessel MA/CT Vessel SD). Airway SNR #1 was calculated using the MA and SD from airway ROI #1, while airway SNR #2 was calculated using the MA and SD from airway ROI #2, and so forth. Third, airway contrast-to-noise ratio (CNR) was calculated for 20 ROI pairs, each consisting of one airway ROI and one muscle ROI, selected sequentially from cranial to caudal direction. Similarly, vessel CNR was calculated for 20 ROI pairs, each consisting of one vessel ROI and one muscle ROI located on the same axial slice. For example, vessel CNR #1 was calculated using the MA from vessel ROI #1, and MA and SD from muscle ROI #1 located on the same axial slice. Vessel CNR #2 was calculated using the MA from vessel ROI #2, and MA and SD from muscle ROI #2 located on the same axial slice, and so forth. The following equations were used to calculate: CNR = (CT Airway MA - CT Muscle MA)/CT Muscle SD and (CT Vessel MA - CT Muscle MA)/CT Muscle SD.

For nodule sharpness, the same scientist set four identical linear lines on each nodule at different angles (horizontal, vertical, right diagonal, and left diagonal). Each line was set on a cross-sectional image and traversed through the center of the GGN, and intensity profiles were plotted for each line (Supplementary Fig. 1). The intensity profile graph was used to calculate the full-width at half-maximum (FWHM) value, with the four FWHM values for each nodule, resulting in 20 measurements for each image dataset.

Subjective Image Quality Assessment

Two board-certified thoracic radiologists, one with 8 years and the other with 16 years of experience in chest CT, visually examined the subjective image quality. The reviewers were blinded to the reconstruction algorithm and radiation dose and unaware of the other radiologist's scoring. The reviewers independently assessed the entire image sets which were in random order. Each dataset was evaluated, and scoring was performed at ten different axial image slices in terms of nodule sharpness, image noise, and overall diagnostic acceptability using a 5-point scale, and image artifacts such as streak artifacts were assessed using a 3-point scale (Supplementary Table 1) [13].

Statistical Analysis

All continuous data was expressed as the mean ± SD. To compare the differences between the reconstruction methods, statistical analysis using repeated measures analysis of variance with Tukey's test as the post hoc test was performed. The subjective image quality values provided by the two reviewers were averaged for the analysis of subjective image quality assessment. Interobserver agreement in the subjective image quality was calculated using Cohen's kappa analysis. A κ-value of <0.20 was considered poor agreement; a κ-value of 0.21–0.40 indicated fair agreement; a κ-value of 0.41–0.60 was moderate agreement; a κ-value of 0.61–0.80 was substantial agreement; and a κ-value of ≥0.81 was excellent agreement [14]. A *P*-value of less than 0.05 was considered statistically significant. All statistical calculations were performed with SPSS (version 26.0; IBM Corp., Armonk, NY, USA).

RESULTS

Radiation Dose

Supplementary Table 2 summarizes the study protocol and radiation doses. The effective radiation dose was 1.7, 0.7, 0.26, and 0.04 mSv for the standard protocol, 120 kVp/25 mAs, 100 kVp/15 mAs, and 80 kVp/5 mAs, respectively.

Comparison of Objective CT Image Quality

As shown in Table 1, the three reconstruction algorithms had significant differences in the mean image noise across the 20 ROIs measured in the fat tissue. AR50 demonstrated

Table 1. Image noise, as measured by SD values of 20 ROIs placed in the fat tissue

Radiation dose	Reconstruction method			*P*			
	AR50 (n = 20 ROIs)	TF (n = 20 ROIs)	TF + Lu (n = 20 ROIs)	*P**	AR50 vs. TF	AR50 vs. TF + Lu	TF vs. TF + Lu
Standard	59.20 ± 7.75	11.41 ± 1.22	37.83 ± 4.58	0.001	0.001	0.001	0.001
120 kVp 25 mAs	77.20 ± 10.27	14.55 ± 1.89	48.76 ± 6.08	0.001	0.001	0.001	0.001
100 kVp 15 mAs	116.60 ± 14.98	22.07 ± 2.89	75.91 ± 9.37	0.001	0.001	0.001	0.001
80 kVp 5 mAs	155.00 ± 26.82	37.13 ± 4.85	118.40 ± 13.39	0.001	0.001	0.001	0.001

The unit of the values is Hounsfield unit and the data are expressed as the mean ± SD.
**P*-values for repeated measures ANOVA. Otherwise indicated, the *P*-values are derived from the post-hoc Tukey's test.
SD = standard deviation, ROIs = regions of interest, AR50 = adaptive statistical iterative reconstruction-V at a level of 50%, TF = Truefidelity, TF + Lu = Truefidelity with a lung enhancement filter

https://doi.org/10.3348/kjr.2024.0472

the highest level of noise, which decreased with the use of TF + Lu and further decreased with the use of TF alone (P = 0.001). This trend remained consistent across all radiation doses. As the radiation dose decreased, the level of the mean image noise increased.

Table 2 displays the SNR at multiple radiation doses and comparison among different reconstruction methods. TF consistently demonstrated higher SNR compared to TF + Lu and AR50 at all levels of radiation exposure. Notably, at the 100 kVp 15 mAs scan for vessel regions, TF + Lu showed better SNR than AR50 (P = 0.037).

Table 3 demonstrates CNR at multiple radiation doses and comparison among different reconstruction methods. TF showed the best CNR, followed by TF + Lu, while AR50 showed the lowest CNR (P = 0.001), except at the lowest radiation dose of 80 kVp 5 mAs. At this lowest radiation dose, TF demonstrated superior CNR when compared to AR50 and TF + Lu, but there was no significant difference between AR50 and TF + Lu.

The nodule sharpness, as measured by FWHM, is shown in Table 4 for multiple radiation doses and compared among different reconstruction methods. TF + Lu significantly improved nodule sharpness at all radiation doses compared to TF alone (Fig. 1). The nodule sharpness of TF + Lu was similar to that of AR50 (Fig. 2). There was no significant difference in nodule sharpness values between different radiation doses when using the same reconstruction algorithm (all P-values > 0.05).

Comparison of Subjective CT Image Quality

Table 5 shows the subjective image quality analysis results for sharpness, noise, artifacts, and overall diagnostic

Table 2. Signal-to-noise ratio for airway and vessel

Radiation	Region	Reconstruction method			*P*			
		AR50 (n = 20 ROIs)	TF (n = 20 ROIs)	TF + Lu (n = 20 ROIs)	P*	AR50 vs. TF	AR50 vs. TF + Lu	TF vs. TF + Lu
Standard	Airway	11.16 ± 1.67	61.15 ± 17.26	17.38 ± 4.23	0.001	0.001	0.093	0.001
	Vessel	0.30 ± 0.14	1.80 ± 0.43	0.47 ± 0.19	0.001	0.001	0.058	0.001
120 kVp 25 mAs	Airway	10.02 ± 1.65	54.96 ± 23.67	15.76 ± 5.68	0.001	0.001	0.260	0.001
	Vessel	0.22 ± 0.10	1.53 ± 0.52	0.40 ± 0.16	0.001	0.001	0.086	0.001
100 kVp 15 mAs	Airway	7.90 ± 1.03	35.04 ± 8.80	10.46 ± 2.34	0.001	0.001	0.150	0.001
	Vessel	0.22 ± 0.11	1.29 ± 0.33	0.37 ± 0.16	0.001	0.001	0.037	0.001
80 kVp 5 mAs	Airway	6.22 ± 1.23	28.40 ± 52.35	6.51 ± 2.57	0.001	0.015	0.999	0.017
	Vessel	0.28 ± 0.16	1.41 ± 0.50	0.40 ± 0.19	0.001	0.001	0.335	0.001

Data are expressed as the mean ± standard deviation.
*P-values for repeated measures ANOVA. Otherwise indicated, the P-values are derived from the post-hoc Tukey's test.
AR50 = adaptive statistical iterative reconstruction-V at a level of 50%, ROIs = regions of interest, TF = Truefidelity, TF + Lu = Truefidelity with a lung enhancement filter

Table 3. Contrast-to-noise ratio for airway and vessel

Radiation	Region	Reconstruction method			*P*			
		AR50 (n = 20 ROI pairs)	TF (n = 20 ROI pairs)	TF + Lu (n = 20 ROI pairs)	P*	AR50 vs. TF	AR50 vs. TF + Lu	TF vs. TF + Lu
Standard	Airway	12.23 ± 1.51	73.57 ± 10.18	20.63 ± 2.23	0.001	0.001	0.001	0.001
	Vessel	0.73 ± 0.15	4.76 ± 0.64	1.30 ± 0.21	0.001	0.001	0.001	0.001
120 kVp 25 mAs	Airway	9.80 ± 1.02	60.50 ± 6.44	16.94 ± 1.69	0.001	0.001	0.001	0.001
	Vessel	0.59 ± 0.10	3.94 ± 0.55	1.09 ± 0.18	0.001	0.001	0.001	0.001
100 kVp 15 mAs	Airway	6.58 ± 0.73	39.11 ± 3.78	10.88 ± 0.89	0.001	0.001	0.001	0.001
	Vessel	0.43 ± 0.13	2.81 ± 0.43	0.76 ± 0.18	0.001	0.001	0.001	0.001
80 kVp 5 mAs	Airway	5.83 ± 0.71	34.99 ± 50.59	7.93 ± 1.01	0.001	0.001	0.958	0.002
	Vessel	0.48 ± 0.16	2.50 ± 0.58	0.69 ± 0.20	0.001	0.001	0.075	0.001

Data are expressed as the mean ± standard deviation.
*P-values for repeated measures ANOVA. Otherwise indicated, the P-values are derived from the post-hoc Tukey's test.
AR50 = adaptive statistical iterative reconstruction-V at a level of 50%, ROIs = regions of interest, TF = Truefidelity, TF + Lu = Truefidelity with a lung enhancement filter

https://doi.org/10.3348/kjr.2024.0472

Korean Journal of Radiology
KJR

Table 4. Nodule sharpness, expressed by full-width at half-maximum

Radiation dose	Reconstruction method			*P*			
	AR50 (n = 20*)	TF (n = 20*)	TF + Lu (n = 20*)	*P*†	AR50 vs. TF	AR50 vs. TF + Lu	TF vs. TF + Lu
Standard	15.16 ± 3.14	19.44 ± 4.26	14.04 ± 2.05	0.001	0.001	0.551	0.001
120 kVp 25 mAs	14.83 ± 2.62	18.37 ± 3.25	14.09 ± 2.04	0.001	0.001	0.658	0.001
100 kVp 15 mAs	14.65 ± 4.11	18.93 ± 4.15	13.44 ± 2.43	0.001	0.001	0.547	0.001
80 kVp 5 mAs	13.62 ± 3.02	18.28 ± 4.28	12.65 ± 2.24	0.001	0.001	0.621	0.001

Data are expressed as the mean ± standard deviation.
*Four measurements for each nodule multiplied by 5 nodules, †*P*-values for repeated measures ANOVA. Otherwise indicated, the *P*-values are derived from the post-hoc Tukey's test.
AR50 = adaptive statistical iterative reconstruction-V at a level of 50%, TF = Truefidelity, TF + Lu = Truefidelity with a lung enhancement filter

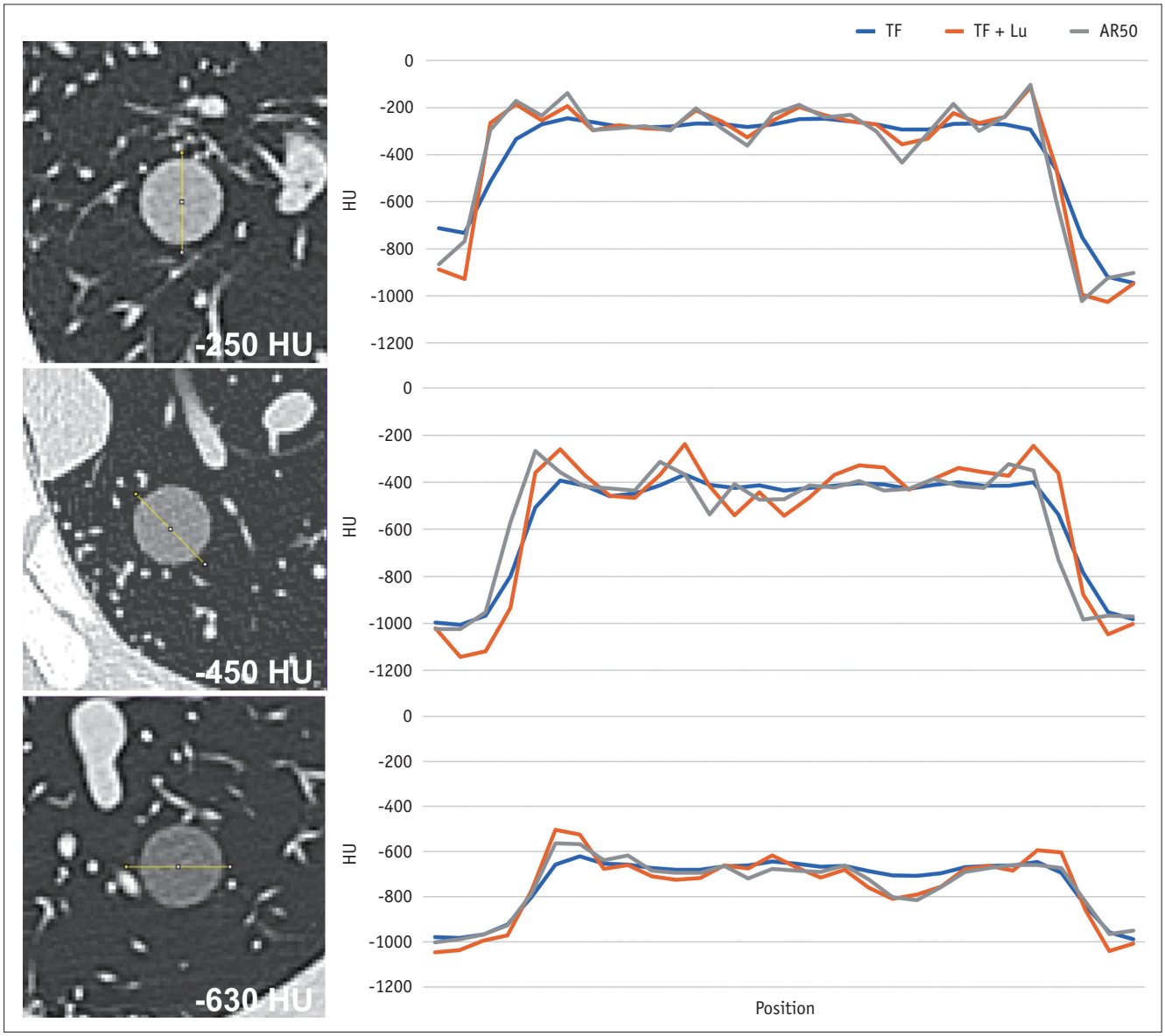

Fig. 1. Comparison of nodule sharpness of three GGNs with densities of -250, -450, and -630 HU, scanned at 120 kVp 25 mAs. Profile curves obtained from the yellow line crossing the center of the nodule demonstrate that TF + Lu improves the nodule sharpness compared to TF alone for all three GGNs. The nodule sharpness of TF + Lu was similar to that of AR50. GGN = ground-glass nodule, HU = Hounsfield unit, TF + Lu = Truefidelity with a lung enhancement filter, TF = Truefidelity, AR50 = adaptive statistical iterative reconstruction-V at a level of 50%

https://doi.org/10.3348/kjr.2024.0472

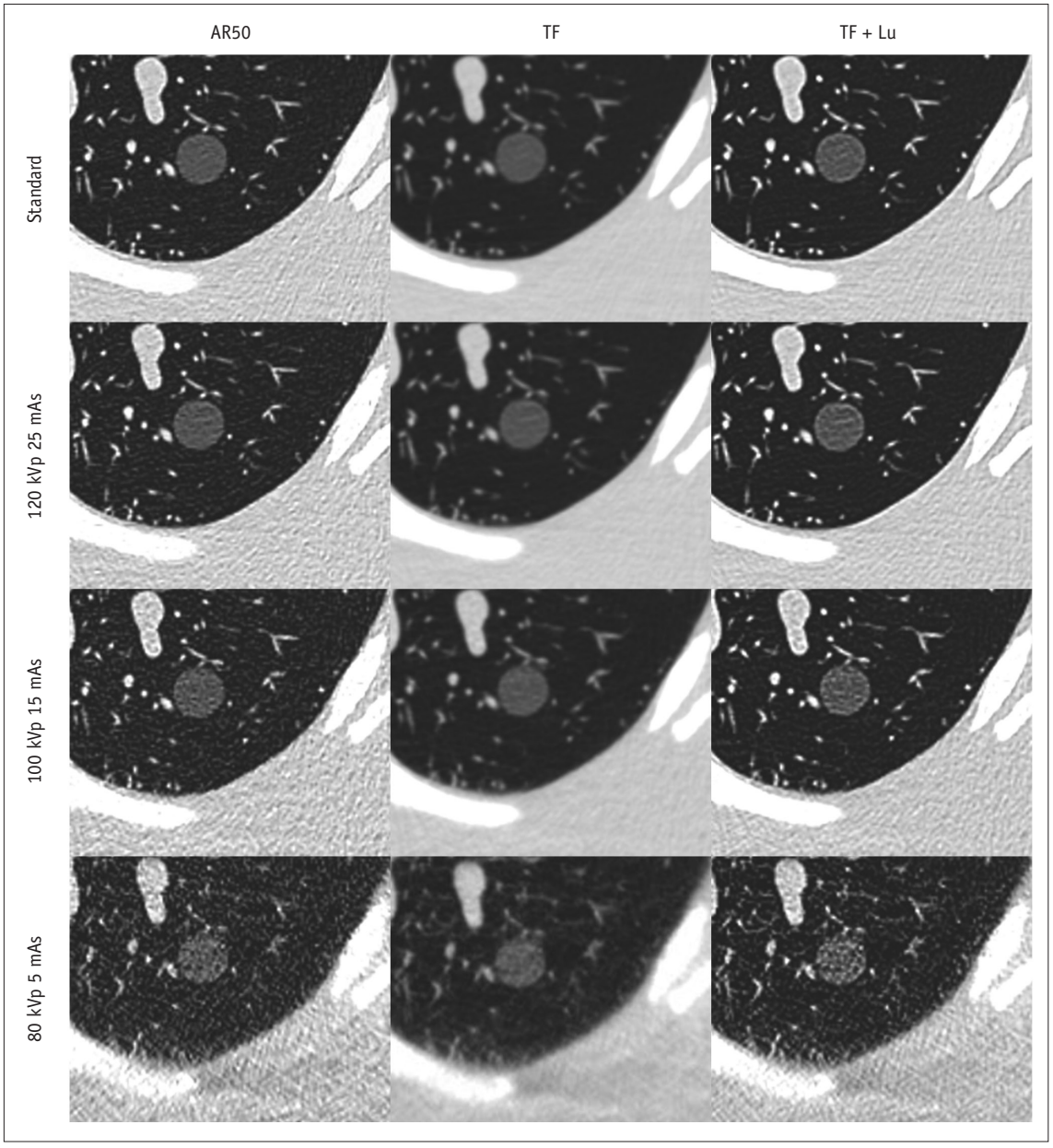

Fig. 2. Images of a ground-glass nodule (10 mm, -630 Hounsfield unit) at four radiation dose settings reconstructed with AR50, TF, and TF + Lu. AR50 = adaptive statistical iterative reconstruction-V at a level of 50%, TF = Truefidelity, TF + Lu = Truefidelity with a lung enhancement filter

acceptability. TF showed significantly better scores for image noise compared to AR50 at all radiation doses (P = 0.001). Nodule sharpness was better with TF + Lu compared to TF at all radiation doses (P = 0.001).

Supplementary Table 3 demonstrates the agreement between the two readers for subjective image quality. According to each subjective image quality parameter, the analysis was moderate to excellent, ranging from 0.574 to 0.818, and according to each reconstruction algorithm, the analysis rated substantial to excellent, ranging from 0.654 to 0.841.

DISCUSSION

Using a lung enhancement filter with DLIR (TF + Lu) significantly increased the sharpness of GGNs at ultralow-dose chest CT scans compared to DLIR alone (TF). Despite some reduction in image quality compared to DLIR alone (TF), incorporating a lung enhancement filter still showed better or similar results to hybrid iterative reconstruction (AR50).

The results of our study are consistent with prior studies, showing that DLIR substantially lowers image noise while

https://doi.org/10.3348/kjr.2024.0472

Korean Journal of Radiology
KJR

Table 5. Subjective image quality analysis results

Radiation dose	Image quality parameters	Reconstruction method			*P*			
		AR50 (n = 10 image slices)	TF (n = 10 image slices)	TF + Lu (n = 10 image slices)	*P**	AR50 vs. TF	AR50 vs. TF + Lu	TF vs. TF + Lu
Standard	Sharpness	5.00 ± 0.00	3.05 ± 0.22	5.00 ± 0.00	0.001	0.001	0.999	0.001
	Noise	4.00 ± 0.00	5.00 ± 0.00	4.45 ± 0.50	0001	0.001	0.025	0.003
	Artifact	3.00 ± 0.00	2.90 ± 0.30	2.95 ± 0.22	0.355	0.999	0.999	0.999
	Overall diagnostic acceptability	5.00 ± 0.00	5.00 ± 0.00	5.00 ± 0.00	0.999	0.999	0.999	0.999
120 kVp 25 mAs	Sharpness	3.95 ± 0.22	3.00 ± 0.00	4.20 ± 0.40	0.001	0.001	0.812	0.001
	Noise	3.95 ± 0.22	5.00 ± 0.00	4.90 ± 0.30	0.001	0.001	0.001	0.999
	Artifact	2.80 ± 0.40	2.85 ± 0.36	2.95 ± 0.22	0.370	0.999	0.999	0.999
	Overall diagnostic acceptability	5.00 ± 0.00	4.85 ± 0.36	5.00 ± 0.00	0.044	0.999	0.999	0.999
100 kVp 15 mAs	Sharpness	3.00 ± 0.00	2.35 ± 0.48	3.00 ± 0.00	0.001	0.001	0.999	0.001
	Noise	3.00 ± 0.00	3.95 ± 0.8	4.00 ± 0.00	0.001	0.001	0.001	0.999
	Artifact	2.70 ± 0.46	2.90 ± 0.30	2.85 ± 0.36	0.241	0.827	0.999	0.999
	Overall diagnostic acceptability	4.00 ± 0.00	3.90 ± 0.30	4.00 ± 0.00	0.131	0.999	0.999	0.999
80 kVp 5 mAs	Sharpness	2.55 ± 0.67	2.05 ± 0.22	3.00 ± 0.00	0.001	0.007	0.096	0.001
	Noise	1.85 ± 0.36	3.60 ± 0.80	2.85 ± 0.36	0.001	0.001	0.001	0.063
	Artifact	1.20 ± 0.40	1.80 ± 0.40	1.30 ± 0.46	0.001	0.001	0.999	0.008
	Overall diagnostic acceptability	2.75 ± 0.43	2.80 ± 0.40	3.50 ± 0.50	0.001	0.999	0.001	0.001

Data are presented as mean ± standard deviation.
**P*-values for repeated measures ANOVA. Otherwise indicated, the *P*-values are derived from the post-hoc Tukey's test.
AR50 = adaptive statistical iterative reconstruction-V at a level of 50%, TF = Truefidelity, TF + Lu = Truefidelity with a lung enhancement filter

increasing both SNR and CNR compared to hybrid iterative reconstruction techniques [15-17]. As the use of traditional filtered back projection shifted to iterative reconstruction a couple of years prior, it may be the trend that iterative reconstruction will move onto DLIR in the near future [18]. Nevertheless, as earlier investigations have noted, the blurred appearance of DLIR may present difficulties in the assessment of GGNs [2,3]. For instance, another study using DLIR from a different vendor with low-dose chest CT found that DLIR effectively reduced image noise and enhanced image quality, similar to our study [19]. However, the study raised concerns about the performance of low-dose chest CT with DLIR in evaluating subsolid nodules and pulmonary emphysema [19]. Notably, this is the first report to compare the performance of a lung enhancement filter with DLIR alone and AR50. We found that image noise and CNR results were between the two reconstruction methods, while SNR was similar to that of AR50.

Another point that should be elaborated is that, the DLIR used in our study is available only with a standard kernel. Substantial reductions in radiation dose when obtaining ultralow or low-dose chest CT scans may increase the image noise and disrupt the margin boundaries, especially GGO components [20,21]. Considering this point, DLIR is valuable because it substantially reduces the image noise and increases image quality. However, when it comes to evaluating GGNs, a lung or sharp kernel is the preferred choice for most radiologists, and current nodule guidelines also advocate using a high-frequency (sharp) kernel [20]. Using a standard kernel to assess GGNs could make the margin ambiguous, precluding accurate margin characterization of especially small GGNs [20]. The lung enhancement filter is designed specifically for efficient filming of lung windows without additional reconstruction time. It enables a reconstruction option to edge enhance anatomical lung structures. Therefore, our study is noteworthy because we demonstrated that DLIR with a lung enhancement filter (TF + Lu) increased the sharpness of GGNs better or similar to AR50 using a lung kernel at ultralow-dose chest CT scans.

The reason why we chose GGNs instead of solid nodules is because the impact of radiation dose and iterative

 https://doi.org/10.3348/kjr.2024.0472

reconstruction type has a more significant effect on GGN measurement than on solid nodules [20,22]. Due to the naturally high contrast with the surrounding lung, solid nodules exhibit more distinct margins and less variability compared to GGNs [23].

Previous studies examining the image quality of different CT reconstruction algorithms usually relied on subjective judgements, with only a few objective measurements such as image noise, SNR, and CNR [24,25]. We assessed both subjective and objective image quality, including FWHM. Some recent studies have used edge-rise distance (ERD) to represent the clarity of edges [2,26,27]. Notably, we used FWHM, which is a numerical measurement of the width of a bump in a curve and is used for segmenting images and identifying edge features [28,29]. Some researchers have used FWHM to measure the edge sharpness of stenosis in coronary arteries across different CT scanners [30,31]. Modifications can be made to this method for its application in future studies on evaluating the image quality of CT scans.

There were several limitations in this study. First, as with any phantom study, the influence and clinical impact of DLIR with a lung enhancement filter on GGNs should be investigated in future human studies. Second, only spherical nodules were used in this study. A future study evaluating nodules with irregular shapes, such as lobulated or spiculated ones, which are more likely to be malignant than spherical nodules, would provide further valuable insights. Third, this study did not consider the effect of heterogeneity in the surrounding lung caused by diseases such as emphysema, pneumonia, or interstitial lung disease. Fourth, we did not compare our FWHM method with other quantitative measurements, such as ERD, that were beyond the scope of this study. However, we believe that similar results would have been obtained in terms of nodule sharpness and spatial resolution among different reconstruction methods. Fifth, due to increased noise in low radiation protocols and the minimal contrast between GGN and neighboring lung tissue, fully automated segmentation was somewhat limited in accurately measuring the volumetry of GGNs. Finally, reconstruction methods from different vendors and various radiation doses may generate discrepancies.

In conclusion, the addition of a lung enhancement filter to DLIR (TF + Lu) significantly improved the nodule sharpness compared to using DLIR alone. DLIR combined with a lung filter (TF + Lu) can be an effective reconstruction technique to enhance image quality and GGN evaluation in ultralow-dose chest CT scans.

Supplement

The Supplement is available with this article at https://doi.org/10.3348/kjr.2024.0472.

Availability of Data and Material

The datasets generated or analyzed during the study are available from the corresponding author on reasonable request.

Conflicts of Interest

The authors have no potential conflicts of interest to disclose.

Author Contributions

Conceptualization: Ji Won Lee, Geewon Lee. Data curation: Shinhyung Kang. Formal analysis: Min-Hee Hwang, Ji Won Lee, Geewon Lee. Funding acquisition: Geewon Lee. Investigation: Min-Hee Hwang, Ji Won Lee, Geewon Lee. Methodology: Min-Hee Hwang, Ji Won Lee, Geewon Lee. Project administration: Shinhyung Kang. Resources: Shinhyung Kang. Software: Shinhyung Kang. Supervision: Geewon Lee. Validation: Shinhyung Kang. Visualization: Geewon Lee. Writing—original draft: Min-Hee Hwang, Ji Won Lee, Geewon Lee. Writing—review & editing: Min-Hee Hwang, Shinhyung Kang, Ji Won Lee, Geewon Lee.

ORCID IDs

Min-Hee Hwang
https://orcid.org/0000-0003-2603-616X
Shinhyung Kang
https://orcid.org/0009-0003-9428-6029
Ji Won Lee
https://orcid.org/0000-0003-1800-8548
Geewon Lee
https://orcid.org/0000-0002-8278-0500

Funding Statement

This work was supported by clinical research grant from Pusan National University Hospital in 2021.

REFERENCES

1. Koetzier LR, Mastrodicasa D, Szczykutowicz TP, van der Werf NR, Wang AS, Sandfort V, et al. Deep learning image

reconstruction for CT: technical principles and clinical prospects. *Radiology* 2023;306:e221257
2. Nam JG, Ahn C, Choi H, Hong W, Park J, Kim JH, et al. Image quality of ultralow-dose chest CT using deep learning techniques: potential superiority of vendor-agnostic post-processing over vendor-specific techniques. *Eur Radiol* 2021;31:5139-5147
3. Svalkvist A, Fagman E, Vikgren J, Ku S, Diniz MO, Norrlund RR, et al. Evaluation of deep-learning image reconstruction for chest CT examinations at two different dose levels. *J Appl Clin Med Phys* 2023;24:e13871
4. National Lung Screening Trial Research Team; Aberle DR, Adams AM, Berg CD, Black WC, Clapp JD, Fagerstrom RM, et al. Reduced lung-cancer mortality with low-dose computed tomographic screening. *N Engl J Med* 2011;365:395-409
5. Kazerooni EA, Armstrong MR, Amorosa JK, Hernandez D, Liebscher LA, Nath H, et al. ACR CT accreditation program and the lung cancer screening program designation. *J Am Coll Radiol* 2016;13(2 Suppl):R30-R34
6. MacMahon H, Naidich DP, Goo JM, Lee KS, Leung ANC, Mayo JR, et al. Guidelines for management of incidental pulmonary nodules detected on CT images: from the Fleischner Society 2017. *Radiology* 2017;284:228-243
7. Bankier AA, MacMahon H, Colby T, Gevenois PA, Goo JM, Leung ANC, et al. Fleischner Society: glossary of terms for thoracic imaging. *Radiology* 2024;310:e232558
8. Remy-Jardin M, Remy J, Giraud F, Wattinne L, Gosselin B. Computed tomography assessment of ground-glass opacity: semiology and significance. *J Thorac Imaging* 1993;8:249-264
9. Hu H, Wang Q, Tang H, Xiong L, Lin Q. Multi-slice computed tomography characteristics of solitary pulmonary ground-glass nodules: differences between malignant and benign. *Thorac Cancer* 2016;7:80-87
10. Nambu A, Araki T, Taguchi Y, Ozawa K, Miyata K, Miyazawa M, et al. Focal area of ground-glass opacity and ground-glass opacity predominance on thin-section CT: discrimination between neoplastic and non-neoplastic lesions. *Clin Radiol* 2005;60:1006-1017
11. Wu F, Tian SP, Jin X, Jing R, Yang YQ, Jin M, et al. CT and histopathologic characteristics of lung adenocarcinoma with pure ground-glass nodules 10 mm or less in diameter. *Eur Radiol* 2017;27:4037-4043
12. Gordic S, Morsbach F, Schmidt B, Allmendinger T, Flohr T, Husarik D, et al. Ultralow-dose chest computed tomography for pulmonary nodule detection: first performance evaluation of single energy scanning with spectral shaping. *Invest Radiol* 2014;49:465-473
13. Park HJ, Choi SY, Lee JE, Lim S, Lee MH, Yi BH, et al. Deep learning image reconstruction algorithm for abdominal multidetector CT at different tube voltages: assessment of image quality and radiation dose in a phantom study. *Eur Radiol* 2022;32:3974-3984
14. Svanholm H, Starklint H, Gundersen HJ, Fabricius J, Barlebo H, Olsen S. Reproducibility of histomorphologic diagnoses with special reference to the kappa statistic. *APMIS* 1989;97:689-698
15. Franck C, Zhang G, Deak P, Zanca F. Preserving image texture while reducing radiation dose with a deep learning image reconstruction algorithm in chest CT: a phantom study. *Phys Med* 2021;81:86-93
16. Jiang B, Li N, Shi X, Zhang S, Li J, de Bock GH, et al. Deep learning reconstruction shows better lung nodule detection for ultra-low-dose chest CT. *Radiology* 2022;303:202-212
17. Kim JH, Yoon HJ, Lee E, Kim I, Cha YK, Bak SH. Validation of deep-learning image reconstruction for low-dose chest computed tomography scan: emphasis on image quality and noise. *Korean J Radiol* 2021;22:131-138
18. Padole A, Ali Khawaja RD, Kalra MK, Singh S. CT radiation dose and iterative reconstruction techniques. *AJR Am J Roentgenol* 2015;204:W384-W392
19. Wang J, Sui X, Zhao R, Du H, Wang J, Wang Y, et al. Value of deep learning reconstruction of chest low-dose CT for image quality improvement and lung parenchyma assessment on lung window. *Eur Radiol* 2024;34:1053-1064
20. Bankier AA, MacMahon H, Goo JM, Rubin GD, Schaefer-Prokop CM, Naidich DP. Recommendations for measuring pulmonary nodules at CT: a statement from the Fleischner Society. *Radiology* 2017;285:584-600
21. Funama Y, Awai K, Liu D, Oda S, Yanaga Y, Nakaura T, et al. Detection of nodules showing ground-glass opacity in the lungs at low-dose multidetector computed tomography: phantom and clinical study. *J Comput Assist Tomogr* 2009;33:49-53
22. Doo KW, Kang EY, Yong HS, Woo OH, Lee KY, Oh YW. Accuracy of lung nodule volumetry in low-dose CT with iterative reconstruction: an anthropomorphic thoracic phantom study. *Br J Radiol* 2014;87:20130644
23. Kubo T, Ohno Y, Takenaka D, Nishino M, Gautam S, Sugimura K, et al. Standard-dose vs. low-dose CT protocols in the evaluation of localized lung lesions: capability for lesion characterization-iLEAD study. *Eur J Radiol Open* 2016;3:67-73
24. Greffier J, Hamard A, Pereira F, Barrau C, Pasquier H, Beregi JP, et al. Image quality and dose reduction opportunity of deep learning image reconstruction algorithm for CT: a phantom study. *Eur Radiol* 2020;30:3951-3959
25. Solomon J, Lyu P, Marin D, Samei E. Noise and spatial resolution properties of a commercially available deep learning-based CT reconstruction algorithm. *Med Phys* 2020;47:3961-3971
26. Hong JH, Park EA, Lee W, Ahn C, Kim JH. Incremental image noise reduction in coronary CT angiography using a deep learning-based technique with iterative reconstruction. *Korean J Radiol* 2020;21:1165-1177
27. Son W, Kim M, Hwang JY, Kim YW, Park C, Choo KS, et al. Comparison of a deep learning-based reconstruction algorithm with filtered back projection and iterative reconstruction algorithms for pediatric abdominopelvic CT. *Korean J Radiol* 2022;23:752-762

 https://doi.org/10.3348/kjr.2024.0472

28. Ohno K, Ohkubo M, Marasinghe JC, Murao K, Matsumoto T, Wada S. Accuracy of lung nodule density on HRCT: analysis by PSF-based image simulation. *J Appl Clin Med Phys* 2012;13:3868
29. Rollo FD, Schulz AG. A contrast efficiency function for quantitatively measuring the spatial-resolution characteristics of scanning systems. *J Nucl Med* 1970;11:53-60
30. Liu LP, Shapira N, Sahbaee P, Gang GJ, Knollman FD, Chen MY, et al. Consistency of spectral results in cardiac dual-source photon-counting CT. *Sci Rep* 2023;13:14895
31. Takafuji M, Kitagawa K, Mizutani S, Hamaguchi A, Kisou R, Iio K, et al. Super-resolution deep learning reconstruction for improved image quality of coronary CT angiography. *Radiol Cardiothorac Imaging* 2023;5:e230085

https://doi.org/10.3348/kjr.2024.0472